International Journal of Pharmaceutics 666 (2024) 124759

Contents lists available at ScienceDirect

International Journal of Pharmaceutics

journal homepage: www.elsevier.com/locate/ijpharm

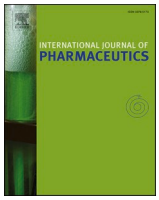

Enhancing Tumor-Specific immunity with SL^{dacA}: A attenuated *Salmonella*-mediated c-di-AMP delivery system targeting the STING pathway

Yuanjia Huang [a], Linghua Piao [b,*], Xiande Liu [a,*]

[a] *School of Life and Health Sciences, Hainan Province Key Laboratory of One Health, Collaborative Innovation center of One Health, Hainan University, No. 58 Renmin Avenue, Haikou 570228, China*

[b] *Key Laboratory of Tropical Translational Medicine of Ministry of Education, School of Basic Medicine and Life Science, Hainan Medical University, No. 3 Xueyuan Avenue, Haikou 57119, China*

A R T I C L E I N F O

Keywords:
STING agonist
Attenuated *Salmonella typhimurium*
c-di-AMP
Dendritic cell maturation
T-cell activation

A B S T R A C T

The STING agonist stimulates an anti-tumor immune response by activating T cells, but its limited tumor-targeting specificity poses risks of cytokine storms or autoimmune reactions. Conversely, attenuated *Salmonella typhimurium* △ppGpp (S.t△ppGpp) exhibits superior tumor-targeting specificity and potent anti-tumor immunogenicity. However, the anti-tumor effects of *Salmonella* carrying STING agonists remain underexplored. In this study, we engineered a strain called SL^{dacA}, utilizing S.t△ppGpp as a carrier, to produce c-di-AMP. This engineered strain effectively enhances dendritic cell maturation and M1-type macrophage polarization by inducing type I interferon production, thereby recruiting and activating effector T cells against tumor progression. This process is regulated by the STING/type I interferon pathway. Our findings indicate that utilizing S.t△ppGpp as a delivery vehicle for STING agonists holds promise as a strategy for synergistic bacterial-mediated immunotherapy.

1. Introduction

Immunotherapy exerts anticancer activity by reprogramming or augmenting immune surveillance and is classified into “passive” methods such as monoclonal antibodies, adoptive T cell transfer, and genetically engineered T cells, or “active” approaches such as cancer vaccines or immune stimulators (Galluzzi et al., 2014). Immunostimulatory therapy, exemplified by its ability to enhance the effectiveness of the immune response, thus facilitating the identification and eradication of tumor cells to inhibit metastasis and recurrence, is adaptable to diverse tumor types (McNutt, 2013). The development of therapeutics mediated by STING has recently emerged as a pivotal avenue in the realm of immunostimulatory therapy. The induction of type I interferons by Antigen Present Cells (APCs) through the STING pathway effectively activates effector T cells, thereby amplifying the anti-tumor immune response (L. k, l. n, y. w, g. h, l. x, c. b, 2022). However, if STING agonists lead to activation of STING in effector T cells, this will lead to apoptosis and ultimately hinder the formation of immune memory (Larkin et al., 2017; Sivick et al., 2018). Furthermore, the lack of tumor-targeted STING agonist therapy raises the potential risk of triggering a systemic inflammatory response, leading to cytokine storms or autoimmune adverse events (Mullard, 2018). Consequently, the development of tumor-targeted delivery options for STING agonists remains a formidable challenge for enhancing their anti-tumor efficacy and mitigating undesirable side effects.

Certain bacteria are actively phagocytosed by APCs and are ideal carriers for the delivery of STING agonists. Bacterial immunotherapy dates back to the mid-19th century, when William Coley used heat-inactivated *Streptococcus pyogenes* and *Serratia marcescens* to treat solid tumors (McCarthy, 2006). Today, bacteria-mediated cancer therapy (BMCT) is recognized as a hopeful approach in the treatment of solid tumors and metastasis. *Salmonella* has been widely studied in this field due to its high tumor specificity, deep tissue penetration, natural bacterial cytotoxicity, ease of genetic modification and safety (Guo et al., 2020). One of the mechanisms for tumor targeting is the disordered blood vessels in tumors result in the creation of oxygen-deprived and necrotic zones, creating perfect settings for essential anaerobic organisms (Duong et al., 2019). In another respect; the nutrients released from

* Corresponding authors.
E-mail addresses: 1342037668@qq.com (L. Piao), 843089676@qq.com (X. Liu).

https://doi.org/10.1016/j.ijpharm.2024.124759
Received 31 May 2024; Received in revised form 20 September 2024; Accepted 24 September 2024
Available online 26 September 2024

necrotic tumor cells, along with bacterial motility and chemokines, support bacterial growth and proliferation. Alternatively, *Salmonella* is forced to invade the tumor for protection after the host inflammation, where the tumor microenvironment is highly immunosuppressive, preventing bacteria from being cleared by the host immune system. Post-tumor infiltration, *Salmonella* infection results in an extensive invasion of immune cells, predominantly neutrophils and dendritic cells, positioned between the tumor's living and necrotic zones, thereby restricting the bacteria's spatial spread (Saccheri et al., 2010; Westphal et al., 2008). Its potential antitumor mechanisms primarily involve inducing autophagy and apoptosis in tumor cells, and it operates by activating host immune cell responses, including neutrophils, macrophages, dendritic cells, $CD4^+$, and $CD8^+$ T cells, thereby inhibiting tumor growth and metastasis (Duong et al., 2019; Guo et al., 2020). To suppress bacterial virulence and make bacteriotherapy safer, some attenuated strains have been constructed. The strain termed ΔppGpp, defective in synthesizing guanosine 5'diphosphate-3′-diphosphate, significantly elevates the median lethal dose (LD50) by a factor of 100,000 to 1,000,000 (Song et al., 2004). The condition is almost non-avirulent in BALB/c mice (Na et al., 2006), exhibiting highly specific tumor targeting and immune activation within the tumor's microenvironment (Kim et al., 2015). Furthermore, S.t△ppGpp has been confirmed as an excellent vector, enhancing the anti-tumor effects of the bacteria by carrying therapeutic payloads, such as Noxa (Jeong et al., 2014); FlaB (Zheng et al., 2017); ClyA (Jiang et al., 2013). Based on these findings, we consider *S. typhimurium* △ppGpp is a promising bacterial vector for STING agonists.

Therefore, we selected S.t△ppGpp as a vector, incorporating the c-di-AMP synthase gene, to explore its anti-tumor effects mediated by the STING signal and its influence on the tumor microenvironment.

2. Materials and methods

2.1. Bacterial strains

Attenuated *Salmonella typhimurium* defective in ΔppGpp synthesis (relA::cat, spoT::kan) (Song et al., 2004), carrying luciferase gene Lux by *P22HT* int transduction, was provided by J. J. Min (Institute for Molecular Imaging and Theranostics, Chonnam National University Hwasun Hospital, Jeonnam, Republic of Korea). The previously described three c-di-AMP synthase genes (dncV, dacA, and cdaS) (Leventhal et al., 2020) was cut with Nco I and Pme I and used to directly replace Rluc8 at the same site in pBAD-pelB-Rluc8 (Le et al., 2011) under the regulatory control of the pBAD promoter.

2.2. Western blot analysis

Protein samples were quantified using a bicinchoninic acid (BCA) assay (Beyotime Technology, China) and separated on sodium dodecyl sulfate–polyacrylamide gels electrophoresis (SDS-PAGE), followed by transfer to nitrocellulose membranes. These membranes were blocked with 5 % Bovine serum albumin (BSA) for 2 h and subsequently incubated with antibodies. The protein bands on the membranes were developed using a super ECL Plus Kit (Boster Biological Technology, Wuhan, China) and recorded by Image Lab software (Tanon 4600SF, Shanghai, China). Anti-Flag antibody was employed to determine gene expression, such as dacA, dncV, and cdaS in bacteria, while anti-p-STING, STING, p-TBK and TBK antibodies were used to determine STING activation in tumors and Anti-β-actin was used as a housekeeping marker. All antibodies were purchased from Bioss Biotechnology (Beijing, China).

2.3. c-di-AMP quantification by HPLC

To quantify CDA production in vitro, bacteria were harvested by centrifugation after induction with L-arabinose (SL^{dacA} group), rinsed with DPBS, 10^{10} cells frozen at − 80 °C. Tumors were harvested from CT26 tumor-bearing mice (as described in *2.4 Mouse tumor models and bacterial injection*) 24 h after L-arabinose injection. Tumors were homogenized in PBS, frozen and stored at − 80 °C. Bacterial pellets, tumor homogenates and c-di-AMP standard (Beijing Psaitong Biotechnology, Beijing, China) were injected into an HPLC system (e2695, Waters, USA) and separated on an X-Bridge C18 column (Waters, USA), with a mobile phase consisting of 0.1 % formic acid (A) and acetonitrile containing 0.1 % formic acid (B). The flow rate was set at 0.8 mL/min, and the column temperature was controlled at 30°C.

2.4. Mouse tumor models and bacterial injection

To establish cancer xenografts, CT26 cells, B16.F10 cells, 4 T1 cells, and HT29 cells (ATCC, VA, USA) were cultured in Dulbecco's Modified Eagle's Medium (DMEM; Gibco, USA) supplemented with 10 % fetal bovine serum (Gibco, USA). CT26 cells (1.5×10^6 cells), 4 T1 cells (1.5×10^6 cells), B16.F10 cells (2×10^5 cells) and HT29 cells (1.5×10^6 cells) were implanted subcutaneously into the right flank of SPF male BALB/c, female BALB/c, male C57BL/6 and BALB/c-nu/nu mice (5–6 weeks old; weighing 18–25 g), respectively. All mice obtained from the Guangdong Medical Laboratory Animal Center (Guangzhou, China). Tumor growth was monitored by measuring their dimensions with a caliper every other day, and tumor volume was calculated using the formula (length × width^2)/2. Once the tumor volume reached 90–160 mm^3, the mice were randomly divided into three groups: phosphate-buffered saline (PBS), S.tΔppGpp/Lux (SL), or S.tΔppGpp/Lux carrying pBAD-pelB-dacA (SL^{dacA}). SL and SL^{dacA} groups were administered 3.75×10^7 colony-forming units (CFU) of bacteria via the tail vein; in addition to bacteria, SL^{dacA} groups were supplemented daily with 0.12 g of L-arabinose via intraperitoneal injection from day 2 to day 16. The STING antagonist, H-151 (MedChemExpress, USA), was administered at 7 μg/kg via intraperitoneal injection on days 3, 5, 7, 9, and 11.

2.5. Bioluminescence imaging

For bacterial monitoring and colonization assessment, CT26 tumor-bearing mice were administered 3.75×10^7 CFU SL or SL^{dacA} by intravenous injection. Starting on day 2, the SL^{dacA} groups were supplemented with 0.12 g L-arabinose daily by intraperitoneal injection. An in vivo imaging system (IVIS 100, Caliper, USA) was used to detect bioluminescence signals generated by Lux in S.t△ppGpp, on days 2, 4, 6 and 8 after administration.

2.6. Bacterial counting

Tissue samples, including heart, liver, spleen, lung, kidney, and tumor, were collected from CT26-tumor-bearing mice on day 3 and day 5 after bacterial administration. These samples were diluted (10-fold) and plated onto LB-agarose plates. After overnight incubation at 37°C, the bacterial titer (CFU/g tissue) was determined using the formula $Y \times 10^Z \times (1 + X) \times 10/X$, where X is the weight of the tissues, Y is the number of colonies on the plate, and Z is the number of times of dilution.

2.7. Hematoxylin and eosin (H&E) staining

The heart, lung, liver, spleen, kidney, and tumor collected from CT26 tumor-bearing mice were fixed in a 4 % paraformaldehyde solution. Paraffin sections (3 μm thick) were prepared and subjected to H&E staining using a commercial staining kit (C0105, Beyotime, China), following the manufacturer's instructions.

2.8. ALT and AST quantification

The sample was detected by mouse serum using alanine transaminase (ALT) and aspartate transaminase (AST) Kits (Shenzhen

Mindray Animal Medical Technology, Shenzhen, China) and analyzed using a Biochemical analyzer (BS-240Vet, Shenzhen Dumbo Medical Technology, Shenzhen, China).

2.9. Real-Time quantitative PCR analysis

To confirm cytokine expression in vivo, tumor tissues from mice were harvested 24 h after L-arabinose injection. RNA isolation from tumors and cells (see *2.10. IFN-1β responses in dendritic cells and THP-1*) was performed using Trizol reagent (Beyotime Biotechnology, China), followed by reverse transcription using the SuperScript II cDNA synthesis kit (Takara, Japan). The qPCR was performed using SYBR Green (Vazyme, Nanjing, China). The HPRT gene was used as a housekeeping gene for BMDC and tumor samples, and the hGAPDH gene was used as the housekeeping gene for THP-1 cells. Primer sequences are listed in Table S1. Relative expression levels compared with control samples were calculated in each experiment using the ΔΔCt method.

2.10. IFN-β responses in dendritic cells, macrophage and THP-1

For the generation of murine bone marrow-derived dendritic cells (BMDC) and bone marrow-derived macrophages (BMDM), bone marrow cells were harvested from the tibia and femur under sterile conditions and erythrocytes were lysed using sterile erythrocyte lysing buffer (Wuhan Servicebio Technology, Co., Ltd.). Bone marrow cells were resuspended in culture medium RPMI 1640-GlutaMax containing 10 % fetal bovine serum, 50 μM 2-mercaptoethanol, penicillin–streptomycin (100 IU/mL and 100 mg/mL) and 20 ng/mL GM-CSF (BioLegend) (in BMDC cultured) or M−CSF (Yeasen) (in BMDM cultured). BMDC were cultured for a further 6 days and BMDM for a further 12 days before use.

Human monocyte THP-1 cells (ATCC, TIB-202) were maintained at 37°C in RPMI supplemented with 10 % fetal bovine serum. 1×10^6 BMDC, BMDM or THP-1 cells/well cells were seeded into a 24 well plate in 0.5 mL without any antibiotics. Bacteria, harvested by centrifugation after induction with L-arabinose (SL^{dacA} group), were added to the plate at MOI of 1 and incubated at 37 °C for 1.5 h to allow internalization of treatments. The cells were washed with PBS containing antibiotics and fresh media containing antibiotics were added. BMDC and BMDM were harvested at 4 h and THP-1 was harvested at 18 h post-treatment. Cells and supernatants were collected for analysis of gene expression and cytokine proteins. Protein levels of IFN-β were determined using ELISA kits purchased from MeiMian (Jiangsu, China) and an Enzyme immunoassay analyzer (Hangzhou Allsheng Instruments Co., Ltd.). mRNA levels of IFN-β were measured using real-time quantitative PCR as described above.

2.11. Flow cytometry analysis

After bacterial stimulation as described above, BMDC were determined by flow cytometry using anti-mouse CD11c/MHC II and CD11c/CD80 antibodies, and BMDM were determined using anti-mouse F4/80 /CD86 and F4/80 /CD206 antibodies. For in vivo experiments, tumor samples were harvested from CT26 tumor-bearing mice 48 h after bacterial administration (as described in *2.4 Mouse tumor models and bacterial injection*). Single cells were isolated from tumor pieces through digestion with collagenase I (Wuhan Servicebio Technology, Co., Ltd.) followed by filtration through a 70 μm cell strainer. The prepared samples were then incubated with specific fluorochrome-labelled antibodies (F4/80, CD86, CD206, Ly6G, CD49b, CD3, CD4, and CD8, Elabscience Biotechnology, Wuhan, China) and analyzed using a FACS Calibur flow cytometer (Beckman Coulter CytoFlex). At least 10,000 events were analyzed in each sample.

2.12. Mass cytometry by time of flight (CyTOF) analysis

Single-cell isolation was performed using the mouse tumor dissociation Kit (130–096-730, Miltenyi Biotec., Germany), and antibody labelling was performed using the Fluidigm labelling kit according to the manufacturer's instructions. For intracellular marker staining, permeabilization buffer (eBioscience, USA) was used according to the manufacturer's instructions. After washing and resuspension, cells were stored at 4°C before acquisition on a Helios instrument (Fluidigm, USA).

2.13. Splenocyte proliferation and T cell polarization

To verify the proliferative and polarizing potential of T cells after BMDC treatment, splenocytes were isolated from the spleen and stained with CFSE. Attenuated *Salmonella*-stimulated BMDC (as described above) were co-cultured with mouse splenocytes at a ratio of 1:10. The samples were subjected to flow cytometry analysis with labelled of CD3, CD4, and CD8 antibodies (Elabscience Biotechnology, Wuhan, China) to measure T cell polarization.

2.14. Data analysis

Statistical analysis was performed using GraphPad Prism software 10. A p-value of less than 0.05 was considered statistically significant. Except for Kaplan-Meier survival analysis was performed log-rank (Mantel-Cox) test, values were compared using one-way ANOVA with Tukey's multiple comparisons posttests. The data were presented as the mean ± standard error of the mean (SEM).

3. Results

3.1. Construction of a c-di-AMP producing system in attenuated Salmonella

Bacterial c-di-AMP has the ability to bind to and activate STING (Krasteva and Sondermann, 2017). To specifically target STING activation within tumor APCs, we utilized S.t△ppGpp (SL) as a vector and developed three attenuated *Salmonella* strains containing the c-di-AMP synthase gene, namely SL^{dncV} (with dncV from *Vibrio cholerae*), SL^{cdas} (with cdaS from *Bacillus subtilis*), and SL^{dacA} (with ^{dacA} from *Listeria monocytogenes*) (Fig. 1A and Figure S1A and B). Western Blot results demonstrated that induction with the plasmid pBAD inducer L-arabinose effectively initiated protein expression (Fig. 1B and Figure S1C, D). However, only SL^{dacA} could produce c-di-AMP after L-arabinose induction, analyzed by HPLC (Fig. 1C, D, E, Figure S1E, F) and matched SL in bacterial abundance (Figure S1G). Similarly, only tumors in SL^{dacA} group showed significant c-di-AMP production (Figure S2). Consequently, we selected SL^{dacA} for the subsequent experiments.

3.2. SL^{dacA} activates $CD4^+$ and $CD8^+$ T cells by enhancing antigen presentation in dendritic cells

Previous studies have shown that *Salmonella* activates dendritic cells (DC) in the tumor microenvironment, thereby increasing the ratio of $CD4^+$ T cells and $CD8^+$ T cells and achieving tumor suppression (Wang et al., 2022). Following initiation of the STING signaling pathway, type I interferons are generated, leading to increased expression of MHC and various co-stimulatory molecules in DC (Weichselbaum et al., 2017; Lan et al., 2014). This process enhances antigen presentation by DC. To investigate the effect of SL^{dacA} on APCs antigen presentation, we infected BMDC, BMDM and THP-1 with SL and SL^{dacA} to assess the ability of APCs to present antigens. The results show that SL^{dacA} significantly increased type I interferon secretion in BMDC (Fig. 2A), BMDM (Figure S4A) and THP-1 (Fig. 2B). Moreover, SL^{dacA} showed upregulation of MHC II ($p < 0.05$, Fig. 2C, D) and the co-stimulatory factor CD80 ($p < 0.001$, Fig. 2E, F) in BMDC compared to the control group, suggesting that SL^{dacA} treatment promotes dendritic cell maturation. To further validate the enhanced antigen presentation ability of BMDC induced by SL^{dacA}, we co-cultured SL^{dacA}-stimulated BMDC with

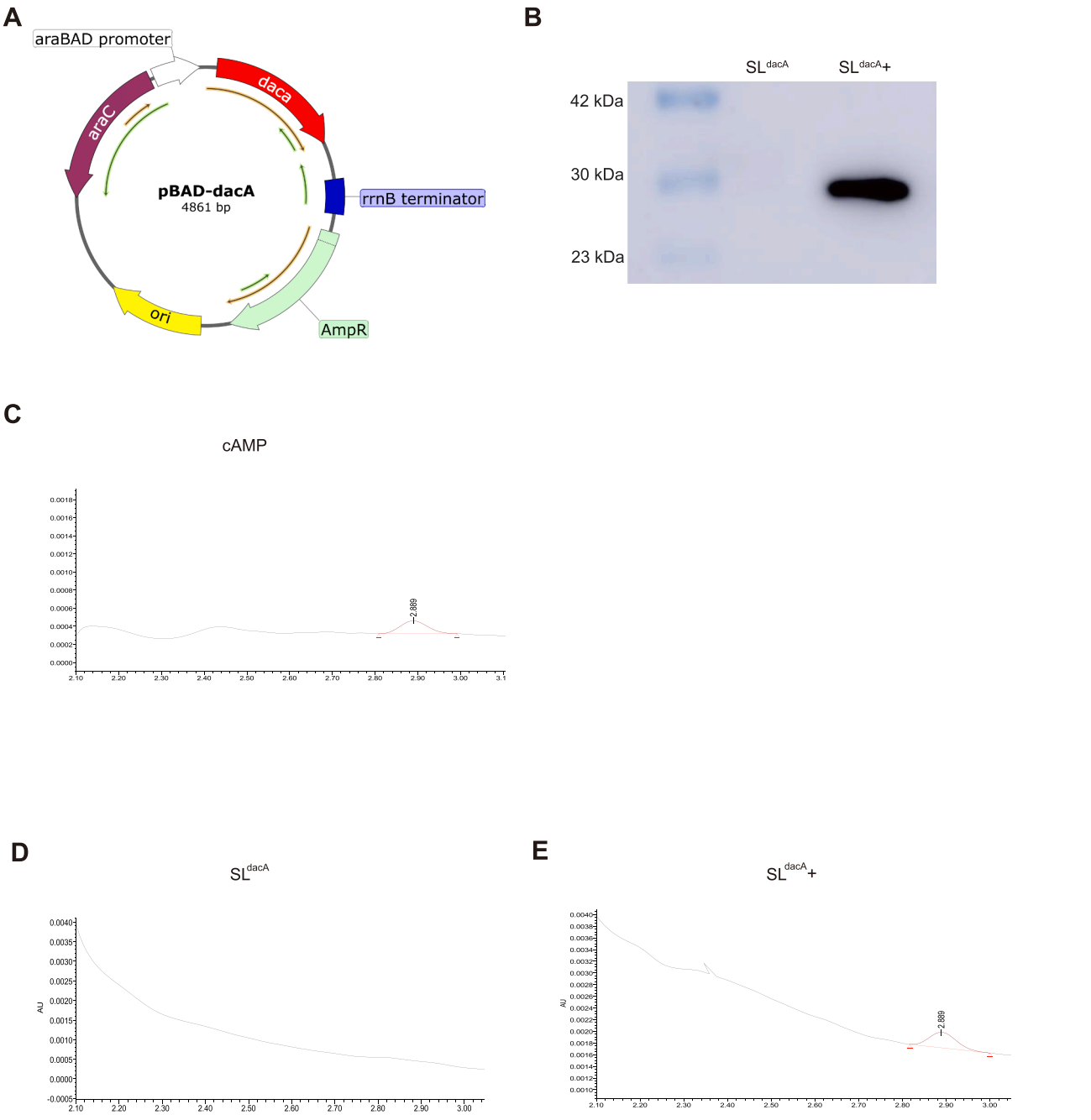

Fig. 1. Expression of dacA by engineered S. typhimurium carrying the pBAD-dacA plasmid(SLdacA). (A) Maps of pBAD-dacA. (B) Expression of dacA in bacteria was analyzed by western blotting with an anti- FLAG antibody without or with (+) induction with 0.2 % L-arabinose. (C) Chromatogram of the c-di-AMP standard. HPLC analysis of the diadenylate cyclase activity of SLdacA without (D) or with (E) induction of 0.2 % L-arabinose.

splenocytes and analyzed the proportion of $CD4^+$ and $CD8^+$ T cells using flow cytometry. Our results indicated that SL^{dacA}-treated BMDC promoted the proliferation of splenocytes ($p < 0.05$, Figure S3A, B) and $CD4^+$ T cells ($p < 0.05$, Figure S3C, D), leading to a significant increase in the proportion of $CD4^+$ and $CD8^+$ T cells ($p < 0.05$, Fig. 2G-J) compared to the control groups. In addition, SL^{dacA} mediated the polarization of M1-type macrophages (Figure S4B-E). These results suggest that SL^{dacA} activates T cells by enhancing the antigen presentation capacity of APCs, which contributes to its antitumor effects.

3.3. SL^{dacA} triggers anti-tumor immunotherapy

To evaluate the anti-tumor activity of SL^{dacA}, we established tumor-bearing mouse models (Fig. 3A). The tumor volumes of mice in the SL^{dacA} treatment group were significantly smaller than those in the control group and the SL treatment group (Fig. 3B, C), and SL and SL^{dacA} do not exhibit any variance in body weight (Fig. 3D). SL^{dacA} resulting in 70 % of mice with complete CT26 tumor rejections (5 of 7) (Fig. 3E). The survival rate of mice was higher in the SL^{dacA} group compared with the SL treatment group (Fig. 3F). Furthermore, the results also indicate that SL^{dacA} significantly inhibits tumor growth and improves survival rates in 4 T1 (Fig. 3G, H and Figure S5C), and B16F10 (Fig. 3I, J and Figure S5D) tumor-bearing mice. Also, there is no difference in the body weight of 4 T1 and B16F10 tumor-bearing mice between SL and SL^{dacA} administration (Figure S5A, B). Together, these results indicate that dacA expression enhances the capacity of SL to fight against cancer.

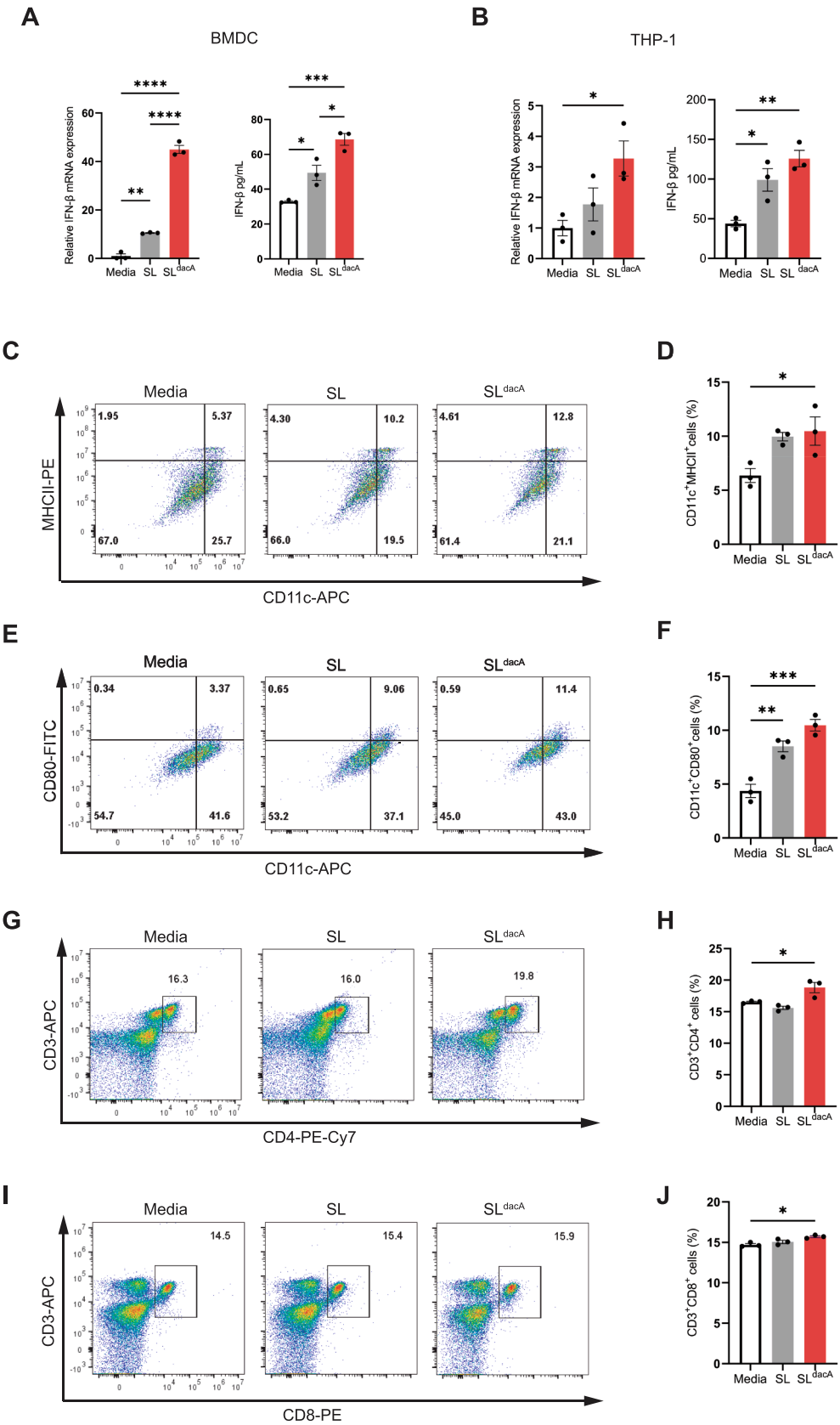

Fig. 2. SLdacA can activate T cells by increasing the antigen presentation capacity of dendritic cells. (A) IFN-β mRNA expression in BMDC and abundance from BMDC supernatants. (B) IFN-β mRNA expression in THP-1 and abundance from THP-1 supernatants. (C) BMDC were double stained with MHCII and CD11c analyzed by Flow Cytometry. (D) CD11c + MHCII + cells statistical graph. (E) BMDC were double stained with CD80 and CD11c analyzed by Flow Cytometry. (F) Histogram for CD11c + CD80 + cells. (G) Splenocyte were double stained with CD3 and CD4 analyzed by Flow Cytometry. (H) Histogram for CD3 + CD4 + cells. (I) splenocyte were double stained with CD3 and CD8 analyzed by Flow Cytometry. (J) Histogram for CD3 + CD8 + cells. Data were expressed as mean ± SEM, n = 3.

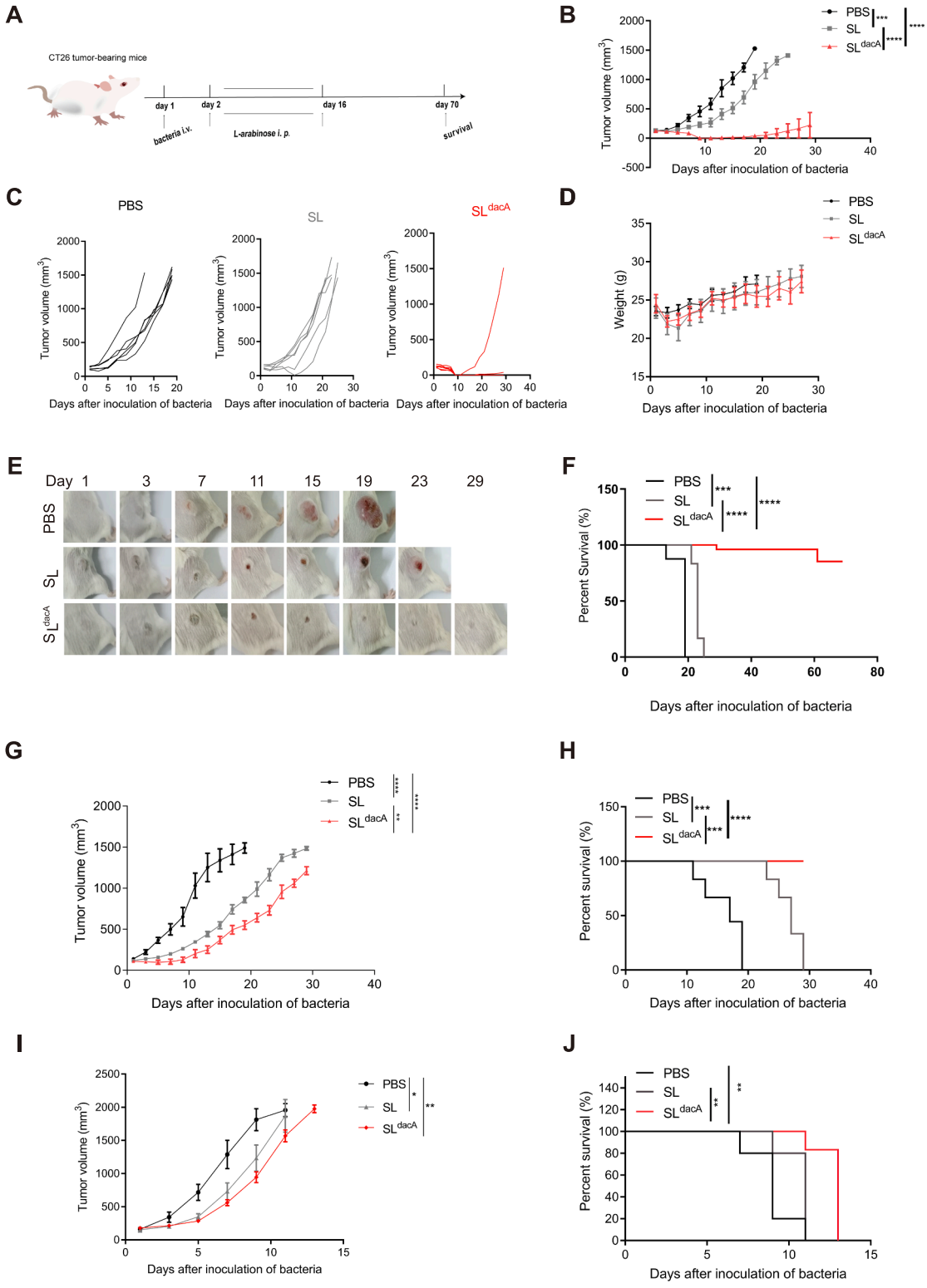

Fig. 3. Anticancer effects of SLdacA in subcutaneous cancer models. (A) Schematic for the treatment of mice. (B) Tumor growth in the CT26 cancer model. (C) CT26 tumors growth in PBS, SL, and SLdacA group respectively, n = 6 for PBS or SL, n = 7 for SLdacA. (D) Changes of mice weight in the CT26 tumor model. (E) Images of CT26 tumor model from representative mice from each group. (G) Tumor growth in the 4 T1 cancer model, n = 5 for PBS, n = 6 for SL and SLdacA. (I) Tumor growth in the B16F10 cancer model, n = 5 for PBS and SL, n = 6 for SLdacA. Mean ± SEM are shown, one-way ANOVA with Tukey's multiple comparisons tests *$p < 0.05$, ** $p < 0.01$, *** $p < 0.001$, **** $p < 0.0001$. (F, H, J) Long-term survival in CT26 tumor-bearing mice (F), 4 T1 tumor-bearing mice (H), or B16F10 tumor-bearing mice (J). Mantel–Cox log-rank comparisons ** $p < 0.01$, *** $p < 0.001$, **** $p < 0.0001$.

3.4. SL^{dacA} has tumor targeting and safety

To investigate the potential impact of c-di-AMP production on tumor-targeting ability, we examined the bioluminescence signal generated by Lux in S.t△ppGpp in the CT26 mouse tumor model of SL and SL^{dacA} group. Our findings revealed that the bioluminescence signal remained detectable in the tumor both in the SL and SL^{dacA} groups until day 8 (Fig. 4A). Furthermore, to explore whether c-di-AMP secretion affects the distribution of SL in major organs, we isolated the heart, liver, spleen, lung, kidney, and tumor from CT26 tumor-bearing mice and conducted viable bacterial counts. The results demonstrated no notable differences in bacterial distribution within the heart, liver, spleen, lung, and kidney between the SL and SL^{dacA} groups on either day 3 or day 5, with the majority of bacteria colonizing at the tumor sites (Fig. 4B). These findings suggest that c-di-AMP production does not impede the tumor-targeting ability of SL.

To evaluate the potential toxicity of SL^{dacA} on major organs, we isolated the heart, liver, spleen, lung, and kidney from CT26 tumor-bearing mice 48 h after bacterial administration, and conducted H&E staining. Our observations indicated that SL^{dacA} administration did not induce any significant pathological abnormalities (Fig. 4C). Furthermore, there were no discernible differences in serum alanine transaminase (ALT) and aspartate transaminase (AST) between the SL^{dacA} and control groups (Fig. 4D). These results affirm that c-di-AMP production does not compromise the tumor-targeting ability of SL and does not elicit adverse effects.

3.5. SL^{dacA} promotes upregulation of pro-inflammatory factor expression in the tumor microenvironment

To investigate the effect of SL^{dacA} on the expression of cytokines in the tumor microenvironment, we examined the mRNA expression of cytokines in tumors from CT26 tumor-bearing mice 48 h after bacterial administration. As shown in Fig. 5, SL^{dacA} significantly upregulated the mRNA expression of IFN-β in the tumor along with its protein expression (Fig. 5A-B, $p < 0.05$). Moreover, SL^{dacA} markedly upregulated pro-inflammatory factors such as IL-6 (Fig. 5C, $p < 0.001$), IL-1β (Fig. 5D, $p < 0.01$), TNF-α (Fig. 5E, $p < 0.01$), PD-L1 (Fig. 5F, $p < 0.001$) and GM-CSF (Fig. 5G, $p < 0.001$). These results indicate that SL^{dacA} can promote an inflammatory response in the tumor microenvironment.

3.6. SL^{dacA} promotes T cells and M1-macrophage infiltration in the tumor microenvironment

To investigate the impact of SL^{dacA} on immune cells within tumors, we utilized flow cytometry to analyze the proportion of $CD4^+$ T cells, $CD8^+$ T cells, M1 macrophages, M2 macrophages, neutrophils, and NK cells in tumors of CT26 tumor-bearing mice 48 h after bacterial administration. As shown in Fig. 6 and Figure S6, SL^{dacA} administration significantly increased the tumor-infiltrating $CD4^+$ T cells ($p < 0.01$, Fig. 6A, B), $CD8^+$ T cells ($p < 0.001$, Fig. 6C, D), and NK cells ($p < 0.01$, Figure S6A, B) compared with the SL group, while reducing the recruitment of neutrophils ($p < 0.0001$, Figure S6C, D). Additionally, compared to the SL group, SL^{dacA} also induced an increase in the proportion of M1 macrophages in the tumor, but not M2 macrophages (Fig. 6E-H). Based on these results, we speculate that SL^{dacA} enhances the anti-tumor effect of SL by further promoting the recruitment of $CD8^+$ T cells, $CD4^+$ T cells, M1 macrophages, and NK cells.

3.7. SL^{dacA} operates by activating T cell and macrophages responses

To precisely identify immune cell phenotypes, we conducted Mass Cytometry analysis on tumor tissues from CT26 tumor-bearing mice 48 h after bacterial administration. The results revealed that SL^{dacA} significantly increased the proportions of T lymphocytes, M1-type macrophages, and NK cells, while neutrophils decreased inversely (Fig. 7A and B, Figure S7A) compared to SL administration. SL^{dacA} upregulated the expression of Ki67 (a cell proliferation marker) in M1 macrophages, T cells, and NK cells (Figure S7B). This is consistent with the results of flow cytometric analysis. Previous studies have shown that STING signaling pathway activation reduces neutrophil aggregation after *Salmonella* induction as assessed by immunofluorescence, whilst contributing to neutrophil polarization to the N1 phenotype and anti-tumor effects (Lu et al., 2024). Our results show that the reduction in neutrophils in the SL^{dacA} group maybe have anti-tumor effects in the same way.

To explore the activation of T cells by SL^{dacA} treatment in vivo, we focused on several T cell activation factors. Markers such as CD25, CD69, ICOS, and CD27 are indicative of T cell activation (Montes-Casado et al., 2020), with CD27 being upregulated in activated $CD8^+$ T cells (Hu et al., 2022). As depicted in Fig. 7C-F, SL^{dacA} upregulated the expression of CD25, CD69, ICOS, and CD27 in T cells compared to the SL group, indicating that SL^{dacA} can promote T cell activation. Additionally, CD80, CD86, and iNOS serve as markers for M1-type macrophages. As shown in Fig. 7G-I, SL^{dacA} upregulated the expression of CD80, CD86, and iNOS in macrophages, suggesting that SL^{dacA} promotes the polarization of M1-type macrophages. Interferons induced by the STING signaling pathway bind to the interferon receptor (IFNAR), activating the Janus kinase (JAK) signaling pathway and subsequently triggering the phosphorylation of STAT1 and STAT2 (Mesev et al., 2019). SL^{dacA} demonstrated an upregulation of pSTAT1 in M1-macrophages, NK cells and T cells. These results indicate that SL^{dacA} exhibits an increase in the polarization of M1-type macrophages and activation of T cells in the tumor environment, possibly associated with the phosphorylation of STAT1.

3.8. SL^{dacA} exerts anti-tumor effects through STING-mediated T cell activation

To confirm the involvement of T cells in the anti-tumor effects of SL^{dacA}, we established HT29 tumor-bearing athymic nude mice. When compared to the SL group and PBS group, SL^{dacA} did not exhibit statistically significant differences in suppressing tumor growth or prolonging the survival time in mice (Fig. 8A, B). This suggests that T cells indeed play a crucial role in the therapeutic efficacy of SL^{dacA}.

To investigate whether SL^{dacA}-mediated upregulation of type I IFN and its anti-tumor activity are linked to the STING signaling pathway in tumor microenvironment, we investigated protein expression of STING, p-STING, TBK, and p-TBK in tumors. Results of Western blotting showed that SL^{dacA} upregulated p-STING/STING and p-TBK/TBK compared with control groups (Figure S8). Subsequently, we treated BMDCs and CT26 tumor-bearing mice with the STING antagonist H-151. The results revealed that H-151 treatment significantly inhibited SL^{dacA}-induced IFN-β secretion in DC cells (Fig. 8C, D) and the anti-tumor effects in CT26 tumor-bearing mice (Fig. 8E, F). These findings highlight a significant association between STING signaling-mediated T cell activation and the anti-tumor effects of SL^{dacA}.

4. Discussion

In this study, we introduced the c-di-AMP-producing enzyme into bacteria, developed three strains—SL^{dncV}, SL^{cdas}, and SL^{dacA}—utilizing *Salmonella typhimurium* ΔppGpp as a vector. However, by HPLC, only SL^{dacA} was found to produce c-di-AMP. Notably, our findings indicate that the delivery of c-di-AMP by SL^{dacA} significantly enhances the anti-tumor efficacy of *S.typhimurium* ΔppGpp in CT26, 4 T1, and B16F10 tumor-bearing mice, with no observed virulence effects. The antitumor effect mediated by *S.typhimurium* ΔppGpp involves two key mechanisms: 1) direct tumor cell-killing through apoptosis or autophagy, correlated with the number and duration of tumor-colonizing bacteria; and 2) activation of effector T cells by dendritic cells (DCs) and macrophages (Liang et al., 2019). Interestingly, we observed that the number and duration of tumor colonization remain unaffected, regardless of

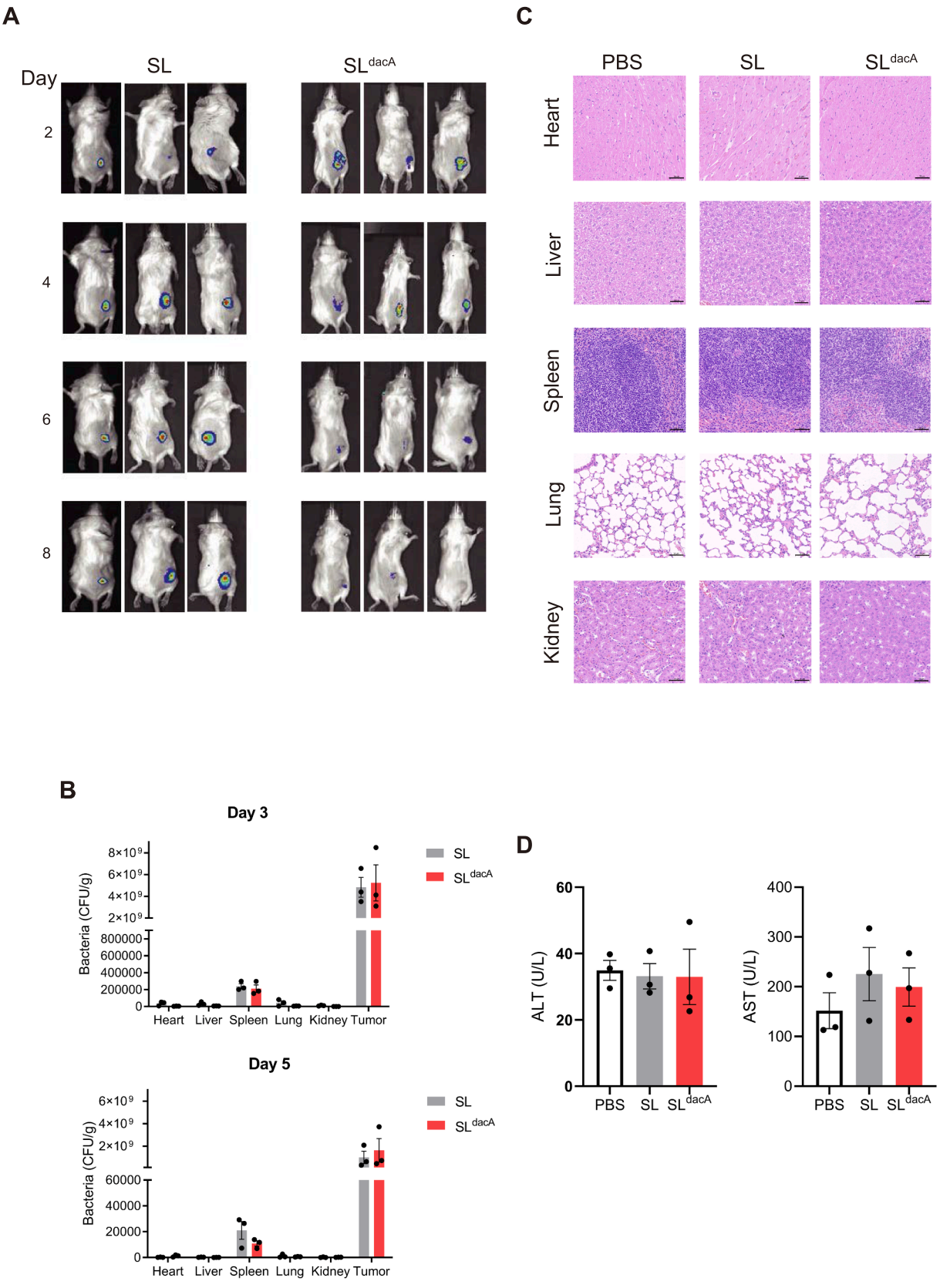

Fig. 4. Targeting and safety analysis of SLdacA in the CT26 cancer model. (A)Non– invasive monitoring of bacterial bioluminescence for 8 days. (B) Bacterial counts in isolated organs from tumor-bearing mice on days 3 and 5. (C) H&E staining for isolated organs of tumor-bearing mice on day 3. Scale bar, 50 mm. (D) AST and ALT levels in the serum were analyzed 3 days post bacterial injection. ALT, alanine transaminase; AST, aspartate transaminase, n = 3.

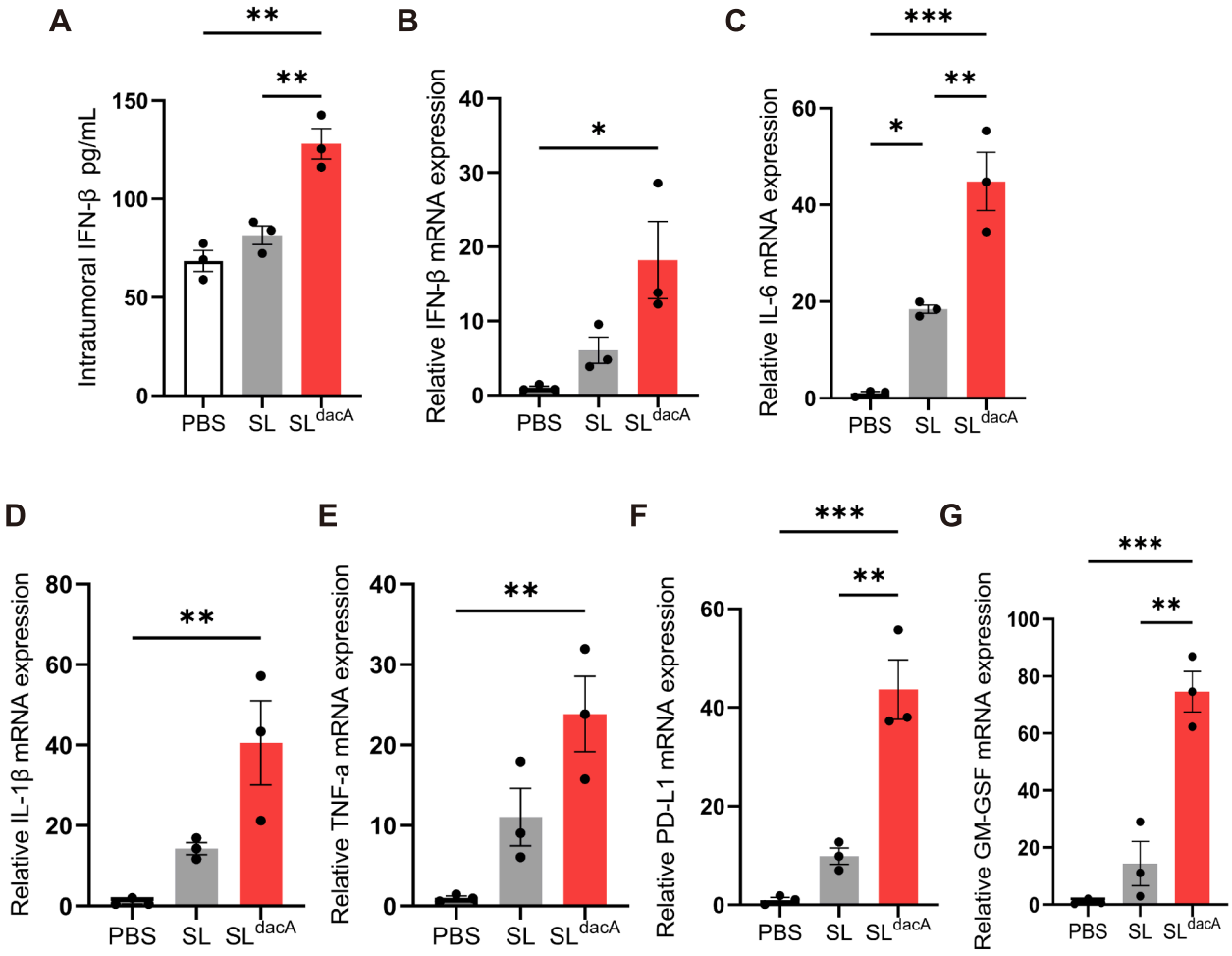

Fig. 5. Expression of cytokines in tumors. (A) IFN-β abundance from tumor supernatants was detected by ELISA. (B-G) Cytokine expression in tumor tissue was detected by qPCR, including IFN-β (B), IL-6 (C), IL-1β (D), TNF-α (E), PD-L1 (F) and GM-CSF (G). Data were expressed as mean ± SEM, n = 3.

whether *Salmonella typhimurium* ΔppGpp produced c-di-AMP or not. Consequently, we hypothesize that the enhanced antitumor activity observed in attenuated *Salmonella* is attributed to the activation of effector T cells by DCs and macrophages through the delivery of c-di-AMP.

To validate our hypothesis, we provided evidence for the role of dendritic cells (DCs) in T cell activation, revealing that SL^{dacA} increased the proportion of $CD11c^{+}MHCII^{+}$ and $CD11c^{+}CD80^{+}$ cells in bone marrow-derived dendritic cells (BMDCs). These matured DCs subsequently contributed to the proportion of $CD4^{+}$ and $CD8^{+}$ T cells in splenocytes. We also observed that SL^{dacA} exhibited an elevated proportion of $CD4^{+}$ and $CD8^{+}$ T cells, along with increased expression of activated markers in tumors such as CD25, CD69, ICOS, and CD27, in comparison to the SL groups. Moreover, SL^{dacA} exhibited elevated expression of activated markers including CD80, CD86, and iNOS, coupled with upregulated cytokines such as IL-1β, TNF-α, IL-6 and GM-CSF, when compared to the SL group. This finding is consistent with a previous study, which indicated that the cytokine GM-CSF stimulates M2-to-M1-type macrophage polarization. M1-type macrophages express costimulatory molecules such as CD80 and CD86, which facilitate efficient T cell priming, thereby supporting the antitumor activity of effector T cells (van Dalen et al., 2018). Finally, we demonstrated that in HT29 tumor-bearing athymic nude mice, the enhanced anti-tumor effect of SL^{dacA} due to T cells was abolished.

STING plays a pivotal role as a crucial link, facilitating the presentation of macrophages and dendritic cells (DCs) to effector T cells by inducing the production of type I interferons (IFNs). Our investigations demonstrated that SL^{dacA} markedly induces the production of type I IFNs in bone marrow-derived dendritic cells (BMDCs), THP-1 macrophages, and tumor tissues obtained from CT26 tumor-bearing mice. Notably, the administration of the STING antagonist, H-151, resulted in the nullification of the enhanced production of type I IFNs in BMDCs, as well as the antitumor effect in CT26-tumor bearing mice, resulting from c-di-AMP delivery by attenuated *Salmonella* SL^{dacA}. Furthermore, it was observed that c-di-AMP delivery by attenuated *Salmonella* SL^{dacA} upregulates STAT1 expression in M1-type macrophages and T cells. This observation is consistent with previous research indicating that the Type I IFNs/STAT1 signaling pathway regulates the polarization of M1-type macrophages (Miao et al., 2020) and the antitumor activity of effector T cells (Xiong et al., 2022). Consequently, we postulate that c-di-AMP delivery by attenuated *Salmonella* mediates the polarization of M1-type macrophages and the activation of effector T cells, likely regulated by the STING-mediated Type I IFNs/STAT1 signaling pathway.

SL^{dacA} has a good anti-tumor effect, not only by recruiting T cells, but also by activating T cells to boost anti-tumor immunity. Administration of SL^{dacA} caused a profound remodeling of the suppressive tumor microenvironment from a 'cold' to a 'hot' state. CT26 is a relatively highly immunogenic tumor model for which SL^{dacA} is more effective (Zuo et al., 2021). SL^{dacA} induced strong tumor remission and enabled the complete eradication of established tumors. Notably; SL^{dacA} also inhibited tumor growth to some extent in 4 T1 and B16F10 tumors, which are considered as immunologically silent and not amenable to ICB

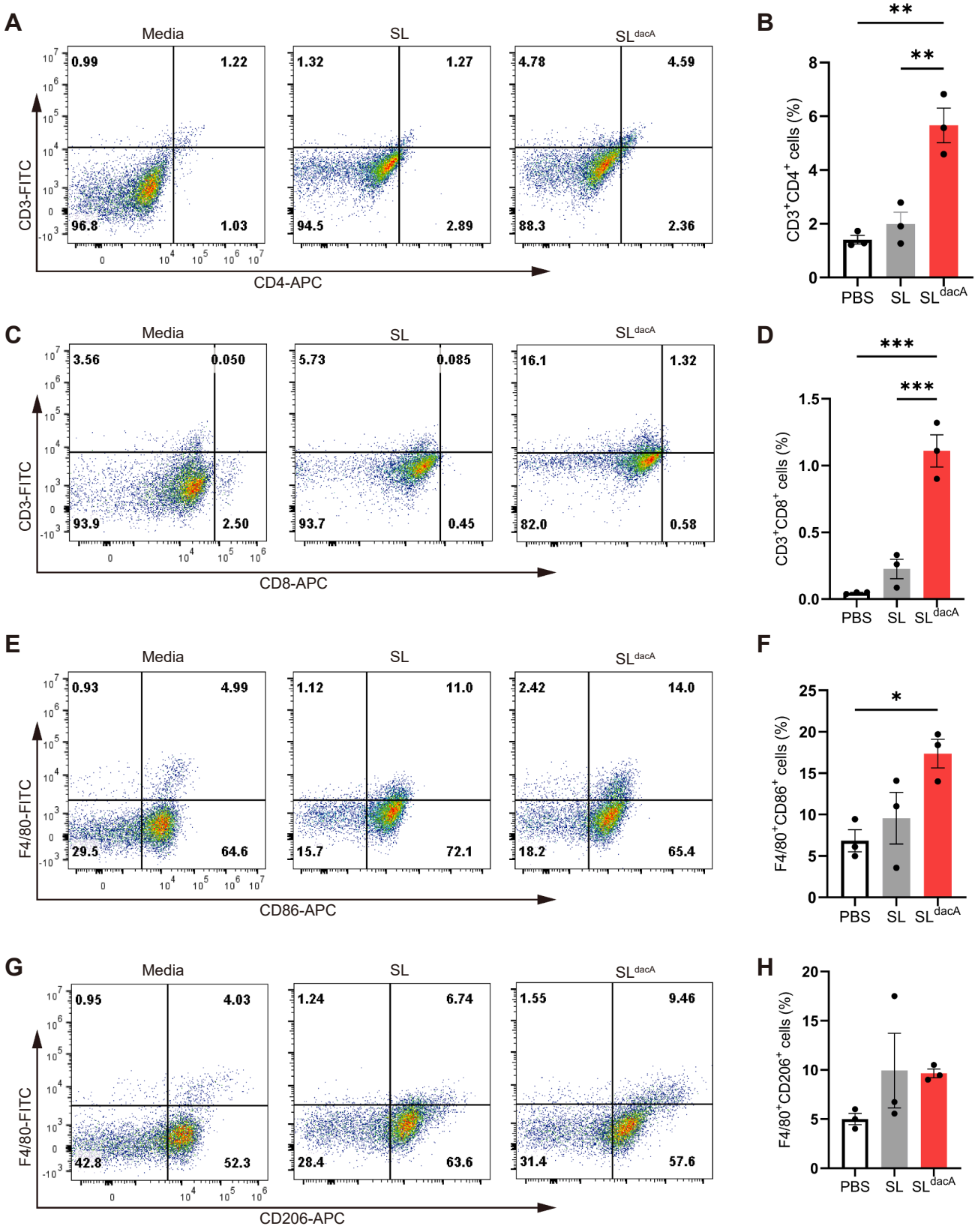

Fig. 6. Effect of SLdacA therapy on tumor-infiltrating T cells and macrophage. (A) Samples were double stained with CD3 and CD4 and analyzed by Flow Cytometry. (B) Histogram for CD3 + CD4 + T cells. (C) Samples were double stained with CD3 and CD8 and analyzed by Flow Cytometry. (D) Histogram for CD3 + CD8 + T cells. (E) Samples were double stained with F4/80 (macrophage marker) and CD86 (M1-type macrophage maker) and analyzed by Flow Cytometry. (F) Histogram for F4/80 + CD86+ (M1-type macrophage). (G) Samples were double stained with F4/80 (macrophage marker) and CD206 (M2-type macrophage maker) and analyzed by Flow Cytometry. (H) Histogram for F4/80 + CD206+ (M2-type macrophage). Data were expressed as mean ± SEM, while n = 3.

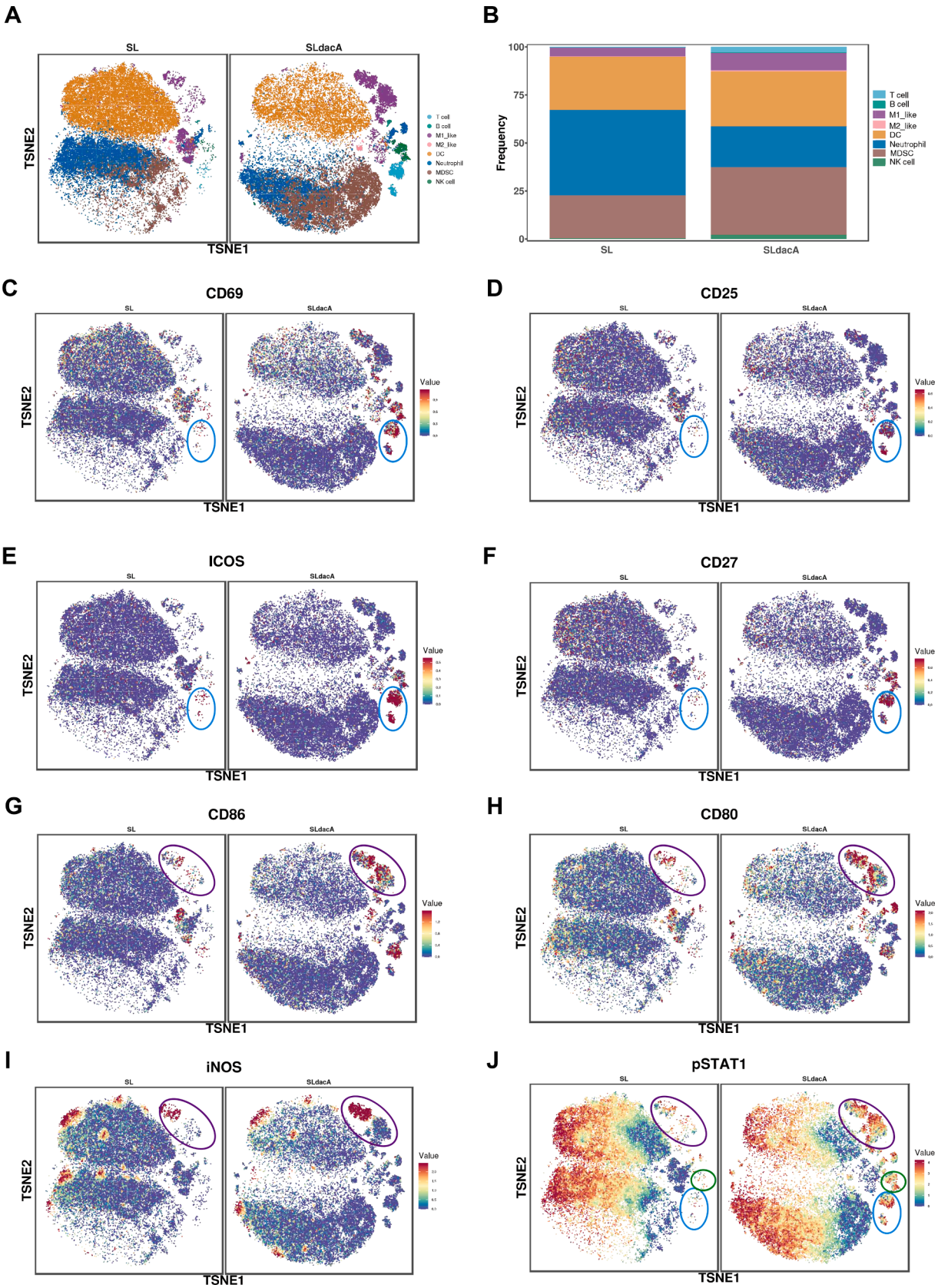

Fig. 7. CyTOF analysis from CT26 tumors given the indicated treatment. (A) The differences in immune composition of the tumor microenvironment between the SL group and the SLdacA group. (B) The distribution proportion of immune cells in the tumor microenvironment of the SL and SLdacA groups. (C-J) t-SNE plots of CD69 (C), CD25(D), ICOS(E), CD27(F), CD86(G), CD80(H), iNOS(I), pSTAT1(J). T cells, M1-type macrophages and NK cells are highlighted by blue, purple and green circles, respectively.

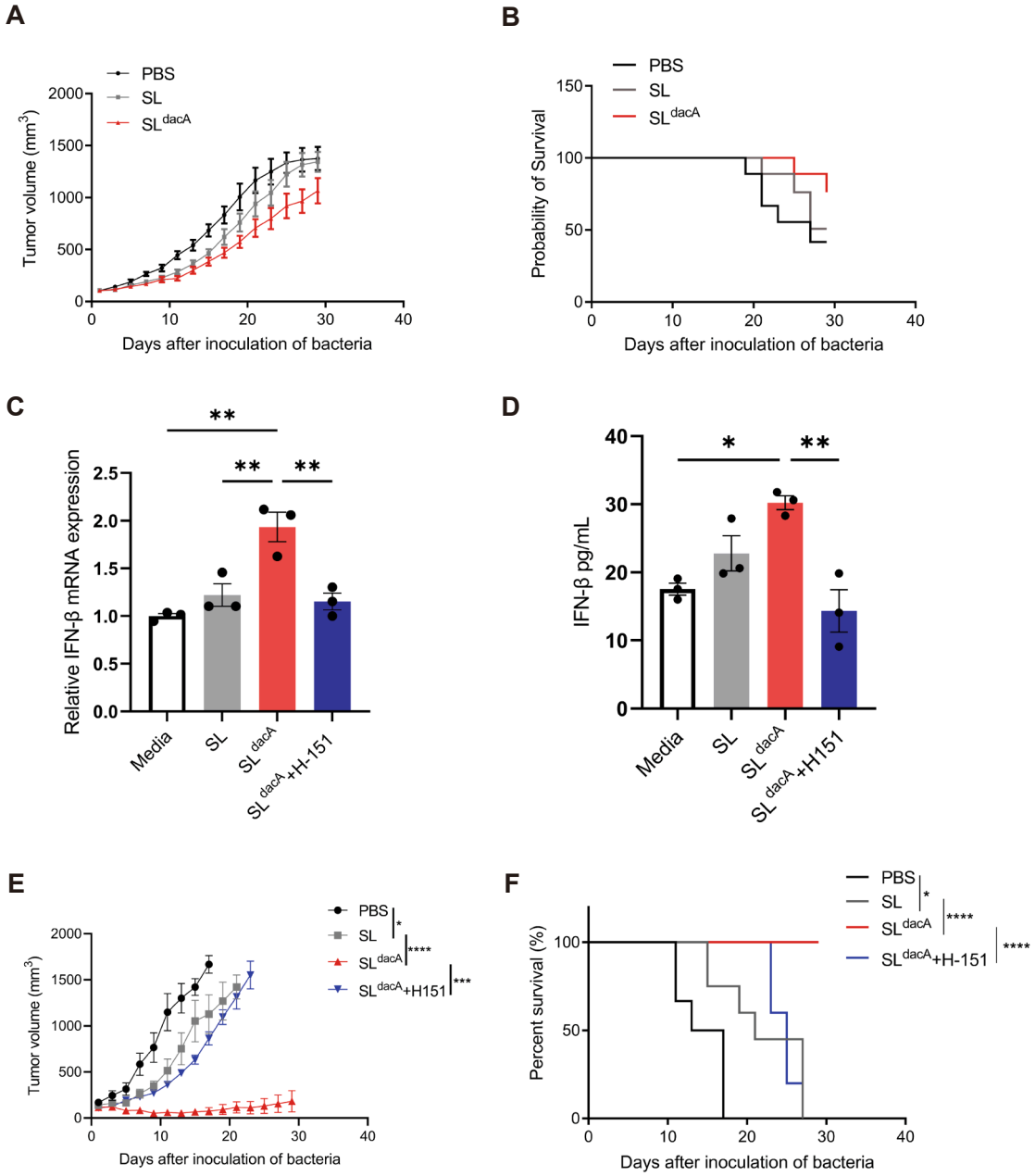

Fig. 8. SLdacA induces tumor-inhibitory responses by stimulating T cell activation through the STING pathway. (A) Tumor growth in HT29 tumor-bearing nude mice. Data were expressed as mean ± SEM, n = 8. (B) Long-term survival for HT29 tumor-bearing nude mice. (C) IFN-β mRNA expression in BMDC was detected by qPCR. (D) IFN-β abundance from BMDC supernatants. (E) Tumor growth curve in CT26 tumor-bearing mice. The data shows the mean ± SEM, n = 8 for SLdacA and n = 5 for other groups. (F) Long-term survival for CT26 tumor-bearing mice. (C-E) One-way ANOVA with Tukey's multiple comparisons *p < 0.05, **p < 0.01, *** p < 0.001, **** p < 0.0001. (F) Mantel–Cox log-rank comparisons *p < 0.05, **** p < 0.0001.

monotherapy (Chen et al., 2023). The first phase of a clinical trial combining cGAS-STING agonists and anti-PD-1 antibody treatment showed encouraging results, with type I IFN induction and reactivated immunotherapy responses in 90.9 % of patients with advanced metastatic solid tumors (Du et al., 2022). As the expression of PD-L1 was upregulated in tumor of the SL^{dacA} group due to activation of STING signaling (He et al., 2023) and inflammatory response in the tumor microenvironment (Taube et al., 2012), combination therapy in combination with PD-L1 antibodies could be considered in future studies to achieve better study outcomes.

Several pathogenic bacteria, such as *Salmonella typhimurium*, *Clostridium novyi*, and *Listeria monocytogenes*, have previously been investigated for cancer immunotherapy due to their inherent tumor-targeting and tumor-killing activities (Duong et al., 2019). While safety remains a major concern, their moderate toxicity enhances direct tumor-killing efficiency and antitumor immune responses in oncolytic bacterial therapies (Kang et al., 2022). Consequently, pathogen-mediated therapeutics necessitate the use of highly attenuated strains. For instance, gene deletions like relA and spot in *S. typhimurium* result in defects in 5′-diphosphate-3′-diphosphate (ppGpp) and lead to a significant increase in the half-lethal dose by 100,1000–1,000,000-fold compared to *S. typhimurium* wild type (Na et al., 2006). Previous studies have demonstrated that this attenuated strain, *S. typhimurium* ΔppGpp, exhibits a similar antitumor effect in vivo but with lower virulence and

higher immune cell infiltration compared to another attenuated strain, VNP20009, which is generated by deleting the msbB and purI genes (Liu et al., 2022). In comparison to *E. coli* MG1655, *S. typhimurium* ΔppGpp stimulates a more robust immune response and the infiltration of macrophages and dendritic cells to suppress tumor progression (Kim et al., 2015). Additionally, various routes such as intratumoral, oral, intravenous, intranasal, and intraperitoneal administration could be utilized in *S. typhimurium* ΔppGpp-based drug delivery (Na et al., 2006). In particular, intravenous administration achieves a more rapid therapeutic effect than other routes due to direct delivery into the systemic circulation without delay (Ruiz et al., 2018). Comparing the findings with BCG-based c-di-AMP delivery by six intravenous administrations (Singh et al., 2022) or *E. coli* Nissle-based c-di-AMP delivery by three intratumoral administrations (Leventhal et al., 2020); *S. typhimurium* ΔppGpp-based c-di-AMP delivery by a single intravenous administration resulted in significant therapeutic effects in tumor-bearing mice. This suggests that *S. typhimurium* ΔppGpp exhibits strong antitumor activity without virulence effects and is adaptable to any route of administration, making it a promising drug delivery carrier for anticancer therapy.

In summary, *S. typhimurium* ΔppGpp-based c-di-AMP delivery enhances the maturation of dendritic cells and the polarization of M1 macrophages through STING-targeted type I IFN production, thereby resulting in effector T cell priming against tumor progression.

Ethics approval and consent to participate

The Hainan University Animal Research Committee approved the animal protocols used in this study.

CRediT authorship contribution statement

Yuanjia Huang: Writing – original draft, Software, Investigation. **Linghua Piao:** Writing – original draft, Investigation. **Xiande Liu:** Writing – review & editing, Project administration, Conceptualization.

Declaration of competing interest

The authors declare that they have no known competing financial interests or personal relationships that could have appeared to influence the work reported in this paper.

Data availability

Data will be made available on request.

Acknowledgments

X. D. L. was supported by the Natural Science Foundation of China (No. 32260854).

Appendix A. Supplementary data

Supplementary data to this article can be found online at https://doi.org/10.1016/j.ijpharm.2024.124759.

References

Chen, X., Meng, F., Xu, Y., Li, T., Chen, X., Wang, H., 2023. Chemically programmed STING-activating nano-liposomal vesicles improve anticancer immunity. Nature Communications 14, 4584.

Du, J.-M., Qian, M.-J., Yuan, T., Chen, R.-H., He, Q.-J., Yang, B., Ling, Q., Zhu, H., 2022. cGAS and cancer therapy: a double-edged sword. Acta Pharmacologica Sinica 43, 2202–2211.

Duong, M.T., Qin, Y., You, S.H., Min, J.J., 2019. Bacteria-cancer interactions: bacteria-based cancer therapy. Exp Mol Med 51, 1–15.

Galluzzi, L., Vacchelli, E., Bravo-San Pedro, J.M., Buqué, A., Senovilla, L., Baracco, E.E., Bloy, N., Castoldi, F., Abastado, J.P., Agostinis, P., Apte, R.N., Aranda, F., Ayyoub, M., Beckhove, P., Blay, J.Y., Bracci, L., Caignard, A., Castelli, C., Cavallo, F., Celis, E., Cerundolo, V., Clayton, A., Colombo, M.P., Coussens, L., Dhodapkar, M.V., Eggermont, A.M., Fearon, D.T., Fridman, W.H., Fučíková, J., Gabrilovich, D.I., Galon, J., Garg, A., Ghiringhelli, F., Giaccone, G., Gilboa, E., Gnjatic, S., Hoos, A., Hosmalin, A., Jäger, D., Kalinski, P., Kärre, K., Kepp, O., Kiessling, R., Kirkwood, J. M., Klein, E., Knuth, A., Lewis, C.E., Liblau, R., Lotze, M.T., Lugli, E., Mach, J.P., Mattei, F., Mavilio, D., Melero, I., Melief, C.J., Mittendorf, E.A., Moretta, L., Odunsi, A., Okada, H., Palucka, A.K., Peter, M.E., Pienta, K.J., Porgador, A., Prendergast, G.C., Rabinovich, G.A., Restifo, N.P., Rizvi, N., Sautès-Fridman, C., Schreiber, H., Seliger, B., Shiku, H., Silva-Santos, B., Smyth, M.J., Speiser, D.E., Spisek, R., Srivastava, P.K., Talmadge, J.E., Tartour, E., Van Der Burg, S.H., Van Den Eynde, B.J., Vile, R., Wagner, H., Weber, J.S., Whiteside, T.L., Wolchok, J.D., Zitvogel, L., Zou, W., Kroemer, G., 2014. Classification of current anticancer immunotherapies. Oncotarget 5, 12472–12508.

Guo, Y., Chen, Y., Liu, X., Min, J.J., Tan, W., Zheng, J.H., 2020. Targeted cancer immunotherapy with genetically engineered oncolytic *Salmonella typhimurium*. Cancer Lett 469, 102–110.

He, X., Sun, Y., Lu, J., Naz, F., Ma, S., Liu, J., 2023. Cytoplasmic DNAs: Sources, sensing, and roles in the development of lung inflammatory diseases and cancer. Front Immunol 14, 1117760.

Hu, B., Yu, M., Ma, X., Sun, J., Liu, C., Wang, C., Wu, S., Fu, P.-Y., Yang, Z., He, Y.-C., Zhu, Y., Huang, C., Yang, X., Shi, Y., Qiu, S., Sun, H., Zhu, A.X., Zhou, J., Xu, Y., Zhu, D., Fan, J., 2022. Interferon-a potentiates anti-PD-1 efficacy by remodeling glucose metabolism in the hepatocellular carcinoma microenvironment. Cancer Discov.

Jeong, J.H., Kim, K., Lim, D., Jeong, K., Hong, Y., Nguyen, V.H., Kim, T.H., Ryu, S., Lim, J.A., Kim, J.I., Kim, G.J., Kim, S.C., Min, J.J., Choy, H.E., 2014. Anti-tumoral effect of the mitochondrial target domain of Noxa delivered by an engineered *Salmonella typhimurium*. PLoS One 9, e80050.

Jiang, S.N., Park, S.H., Lee, H.J., Zheng, J.H., Kim, H.S., Bom, H.S., Hong, Y., Szardenings, M., Shin, M.G., Kim, S.C., Ntziachristos, V., Choy, H.E., Min, J.J., 2013. Engineering of bacteria for the visualization of targeted delivery of a cytolytic anticancer agent. Mol. Ther. 21, 1985–1995.

Kang, S.R., Nguyen, D.H., Yoo, S.W., Min, J.J., 2022. Bacteria and bacterial derivatives as delivery carriers for immunotherapy. Advanced Drug Delivery Reviews 181, 114085.

Kim, J.-E., Phan, T.X., Nguyen, V.H., Dinh-Vu, H.-V., Zheng, J.H., Yun, M., Park, S.-G., Hong, Y., Choy, H.E., Szardenings, M., Hwang, W., Park, J.-A., Park, S., Im, S.-H., Min, J.-J., 2015. *Salmonella typhimurium* suppresses tumor growth via the pro-inflammatory cytokine interleukin-1β. Theranostics 5, 1328–1342.

Krasteva, P., Sondermann, H., 2017. Versatile modes of cellular regulation via cyclic dinucleotides. Nat. Chem. Biol. 13, 350–359.

L. k, l. n, y. w, g. h, l. x, c. b,, 2022. Activation of Stimulation of Interferon Genes (STING) Signal and Cancer Immunotherapy, Molecules (Basel. Switzerland) 27.

Lan, Y.Y., Londoño, D., Bouley, R., Rooney, M.S., Hacohen, N., 2014. Dnase2a deficiency uncovers lysosomal clearance of damaged nuclear DNA via autophagy. Cell Rep. 9, 180–192.

Larkin, B., Ilyukha, V., Sorokin, M., Buzdin, A., Vannier, E., Poltorak, A., 2017. Cutting edge: activation of STING in T cells induces type I IFN responses and cell death. J Immunol 199, 397–402.

Le, U.N., Kim, H.S., Kwon, J.S., Kim, M.Y., Nguyen, V.H., Jiang, S.N., Lee, B.I., Hong, Y., Shin, M.G., Rhee, J.H., Bom, H.S., Ahn, Y., Gambhir, S.S., Choy, H.E., Min, J.J., 2011. Engineering and visualization of bacteria for targeting infarcted myocardium. Molecular Therapy: the Journal of the American Society of Gene Therapy 19, 951–959.

Leventhal, D.S., Sokolovska, A., Li, N., Plescia, C., Kolodziej, S.A., Gallant, C.W., Christmas, R., Gao, J.R., James, M.J., Abin-Fuentes, A., Momin, M., Bergeron, C., Fisher, A., Miller, P.F., West, K.A., Lora, J.M., 2020. Immunotherapy with engineered bacteria by targeting the STING pathway for anti-tumor immunity. Nature Communications 11, 2739.

Liang, K., Liu, Q., Li, P., Luo, H., Wang, H., Kong, Q., 2019. Genetically engineered *Salmonella Typhimurium*: Recent advances in cancer therapy. Cancer Letters 448, 168–181.

Liu, X., Guo, Y., Sun, Y., Chen, Y., Tan, W., Min, J.J., Zheng, J.H., 2022. Comparison of anticancer activities and biosafety between *Salmonella enterica Serovar Typhimurium* ΔppGpp and VNP20009 in a murine cancer model. Front Microbiol 13, 914575.

Lu, S., Mi, Z., Liu, P., Ding, J., Ma, Y., Yang, J., Rong, P., Zhou, W., 2024. Repolarizing neutrophils via MnO_2 nanoparticle-activated STING pathway enhances *Salmonella*-mediated tumor immunotherapy. J Nanobiotechnol 22, 443.

McCarthy, E.F., 2006. The toxins of William B. Coley and the treatment of bone and soft-tissue sarcomas. Iowa Orthop J 26, 154–158.

McNutt, M., 2013. Cancer immunotherapy. Science 342, 1417.

Mesev, E.V., LeDesma, R.A., Ploss, A., 2019. Decoding type I and III interferon signalling during viral infection. Nat Microbiol 4, 914–924.

Miao, L., Qi, J., Zhao, Q., Wu, Q.N., Wei, D.L., Wei, X.L., Liu, J., Chen, J., Zeng, Z.L., Ju, H.Q., Luo, H.Y., Xu, R.H., 2020. Targeting the STING pathway in tumor-associated macrophages regulates innate immune sensing of gastric cancer cells. Theranostics 10, 498–515.

Montes-Casado, M., Sanvicente, A., Casarrubios, L., Feito, M.J., Rojo, J.M., Vallet-Regí, M., Arcos, D., Portolés, P., Portolés, M.T., 2020. An immunological approach to the biocompatibility of mesoporous SiO2-CaO nanospheres. Int. J. Mol. Sci. 21, 8291.

Mullard, A., 2018. Can innate immune system targets turn up the heat on 'cold' tumours? Nature Reviews Drug Discovery 17, 3–5.

Na, H.S., Kim, H.J., Lee, H.-C., Hong, Y., Rhee, J.H., Choy, H.E., 2006. Immune response induced by *Salmonella typhimurium* defective in ppGpp synthesis. Vaccine 24, 2027–2034.

Ruiz, M.E., Ruiz, M.E., Montoto, S.S., 2018. Routes of Drug Administration.

Saccheri, F., Pozzi, C., Avogadri, F., Barozzi, S., Faretta, M., Fusi, P., Rescigno, M., 2010. Bacteria-induced gap junctions in tumors favor antigen cross-presentation and antitumor immunity. Sci Transl Med 2, 44ra57.

Singh, A.K., Praharaj, M., Lombardo, K.A., Yoshida, T., Matoso, A., Baras, A.S., Zhao, L., Srikrishna, G., Huang, J., Prasad, P., Powell, J.D., Kates, M., McConkey, D., Pardoll, D.M., Bishai, W.R., Bivalacqua, T.J., 2022. Re-engineered BCG overexpressing cyclic di-AMP augments trained immunity and exhibits improved efficacy against bladder cancer. Nat Commun 13, 878.

Sivick, K.E., Desbien, A.L., Glickman, L.H., Reiner, G.L., Corrales, L., Surh, N.H., Hudson, T.E., Vu, U.T., Francica, B.J., Banda, T., Katibah, G.E., Kanne, D.B., Leong, J.J., Metchette, K., Bruml, J.R., Ndubaku, C.O., McKenna, J.M., Feng, Y., Zheng, L., Bender, S.L., Cho, C.Y., Leong, M.L., van Elsas, A., Dubensky, T.W., McWhirter, S.M., 2018. Magnitude of therapeutic STING activation determines CD8 + T cell-mediated anti-tumor immunity. Cell Reports 25, 3074–3085.e3075.

Song, M., Kim, H.-J., Kim, E.Y., Shin, M., Lee, H.C., Hong, Y., Rhee, J.H., Yoon, H., Ryu, S., Lim, S., Choy, H.E., 2004. ppGpp-Dependent stationary phase induction of genes on salmonella pathogenicity island. Journal of Biological Chemistry 279, 34183–34190.

Taube, J.M., Anders, R.A., Young, G.D., Xu, H., Sharma, R., McMiller, T.L., Chen, S., Klein, A.P., Pardoll, D.M., Topalian, S.L., Chen, L., 2012. Colocalization of inflammatory response with B7–H1 expression in human melanocytic lesions supports an adaptive resistance mechanism of immune escape. Science Translational Medicine 4, 127ra137.

van Dalen, F.J., van Stevendaal, M., Fennemann, F.L., Verdoes, M., Ilina, O., 2018. Molecular repolarisation of tumour-associated macrophages. Molecules 24.

Wang, W., Xu, H., Ye, Q., Tao, F., Wheeldon, I., Yuan, A., Hu, Y., Wu, J., 2022. Systemic immune responses to irradiated tumours via the transport of antigens to the tumour periphery by injected flagellate bacteria. Nature Biomedical Engineering 6, 44–53.

Weichselbaum, R.R., Liang, H., Deng, L., Fu, Y.X., 2017. Radiotherapy and immunotherapy: a beneficial liaison? Nat. Rev. Clin. Oncol. 14, 365–379.

Westphal, K., Leschner, S., Jablonska, J., Loessner, H., Weiss, S., 2008. Containment of tumor-colonizing bacteria by host neutrophils. Cancer Res 68, 2952–2960.

Xiong, X., Chen, S., Shen, J., You, H., Yang, H., Yan, C., Fang, Z., Zhang, J., Cai, X., Dong, X., Kang, T., Li, W., Zhou, P., 2022. Cannabis suppresses antitumor immunity by inhibiting JAK/STAT signaling in T cells through CNR2. Signal Transduct Target Ther 7, 99.

Zheng, J.H., Nguyen, V.H., Jiang, S.N., Park, S.H., Tan, W., Hong, S.H., Shin, M.G., Chung, I.J., Hong, Y., Bom, H.S., Choy, H.E., Lee, S.E., Rhee, J.H., Min, J.J., 2017. Two-step enhanced cancer immunotherapy with engineered *Salmonella typhimurium* secreting heterologous flagellin. Sci. Transl. Med. 9.

Zuo, S., Wei, M., Xu, T., Kong, L., He, B., Wang, S., Wang, S., Wu, J., Dong, J., Wei, J., 2021. An engineered oncolytic vaccinia virus encoding a single-chain variable fragment against TIGIT induces effective antitumor immunity and synergizes with PD-1 or LAG-3 blockade. J Immunother Cancer 9.